

# Gamma and the Coordination of Spiking Activity in Early Visual Cortex

Xiaoxuan Jia,<sup>1,3,\*</sup> Seiji Tanabe,<sup>1</sup> and Adam Kohn<sup>1,2,\*</sup>

<sup>1</sup>Dominick Purpura Department of Neuroscience

<sup>2</sup>Department of Ophthalmology and Vision Sciences

Albert Einstein College of Medicine, Bronx, NY 10461, USA

<sup>3</sup>Present address: McGovern Institute for Brain Research, Massachusetts Institute of Technology, Cambridge, MA 02139, USA

\*Correspondence: [jxiaoxuan@gmail.com](mailto:jxiaoxuan@gmail.com) (X.J.), [adam.kohn@einstein.yu.edu](mailto:adam.kohn@einstein.yu.edu) (A.K.)

<http://dx.doi.org/10.1016/j.neuron.2012.12.036>

## SUMMARY

Gamma components of the local field potential (LFP) are elevated during cognitive and perceptual processes. It has been suggested that gamma power indicates the strength of neuronal population synchrony, which influences the relaying of signals between cortical areas. However, the relationship between coordinated spiking activity and gamma remains unclear, and the influence on corticocortical signaling largely untested. We investigated these issues by recording from neuronal populations in areas V1 and V2 of anesthetized macaque monkeys. We found that visual stimuli that induce a strong, coherent gamma rhythm result in enhanced pairwise and higher-order V1 synchrony. This is associated with stronger coupling of V1-V2 spiking activity, in a retinotopically specific manner. Coupling is more strongly related to the gamma modulation of V1 firing than to the downstream V2 rhythm. Our results thus show that elevated gamma power is associated with stronger coordination of spiking activity both within and between cortical areas.

## INTRODUCTION

Gamma band (~30–50 Hz) activity has been proposed to be an important coding mechanism in the brain. One suggestion posits that gamma-band spiking activity links the distributed representation of sensory stimuli within a cortical area (Gray et al., 1989). Under this view, the coordination of ensemble spiking activity in the gamma band leads to more effective drive to downstream networks (Singer, 1999). A related, but distinct, proposal is that gamma routes signals between neuronal populations, particularly those in distinct cortical areas. For instance, the “communication through coherence” proposal suggests that the efficacy of synaptic input to a target area can be modulated by its timing relative to the phase of the local gamma cycle (Fries, 2009). The activity of local inhibitory neurons is known to fluctuate rhythmically within a gamma cycle (Hasenstaub et al., 2005; Atallah and Scanziani, 2009), so efficacy should be maximal for inputs

arriving at a gamma phase when inhibition is weakest relative to excitation in the target area.

Early studies in visual cortex focused on spiking activity and provided evidence both for and against gamma modulation (Gray, 1999; Singer, 1999). Recent studies have used gamma power in the local field potential (LFP) and the coupling between the LFP and spiking activity in individual neurons as a potentially more sensitive measurement of shared, weak fluctuations in a distributed neuronal population (Fries et al., 2001; Pesaran et al., 2002; Fries et al., 2008; Gregoriou et al., 2009). However, how altered LFP-based measurements reflect the temporal coordination of spiking responses in a distributed neuronal population remains unclear. Because only a small fraction of LFP power is in the gamma band, altered gamma power or LFP-spike coupling may not indicate a substantial change in spike timing coordination. Further, neurons in a distributed population may have different phase relationships to gamma or be modulated in different epochs, reducing ensemble coordination. Since spikes relay signals between networks, it is necessary to understand how LFP-based measurements are related to the coordination of spiking activity in a distributed neuronal ensemble.

A second issue is whether gamma-coordination can be significant enough to affect the relaying of signals to distant networks. Cortical recordings have shown conditions under which interareal field-field or spike-field coupling is elevated (Frien et al., 1994; Buschman and Miller, 2007; Gregoriou et al., 2009). How this is reflected in the coordination of population spiking responses in distinct cortical areas is largely unknown, as is the relative importance of gamma fluctuations in the source and target areas. Modeling studies suggest that synchrony can enhance signal transmission (Salinas and Sejnowski, 2001; Akam and Kullmann, 2010), but it is not clear whether the coordination they assume is similar in strength to that observed in cortical networks.

Here, we study the relationship between LFP gamma power and the coordination of intra- and interareal spiking activity in early visual cortex. We recorded LFPs and spiking activity in the superficial layers of primary visual cortex (V1) using micro-electrode arrays, and used manipulations of stimulus size and orientation to modulate gamma in a parametric manner. We find that when gamma power is elevated and more spatially coherent, this is associated with stronger gamma-modulation of spiking activity and enhanced pairwise and higher order synchrony. To test the consequence of this coordination, we

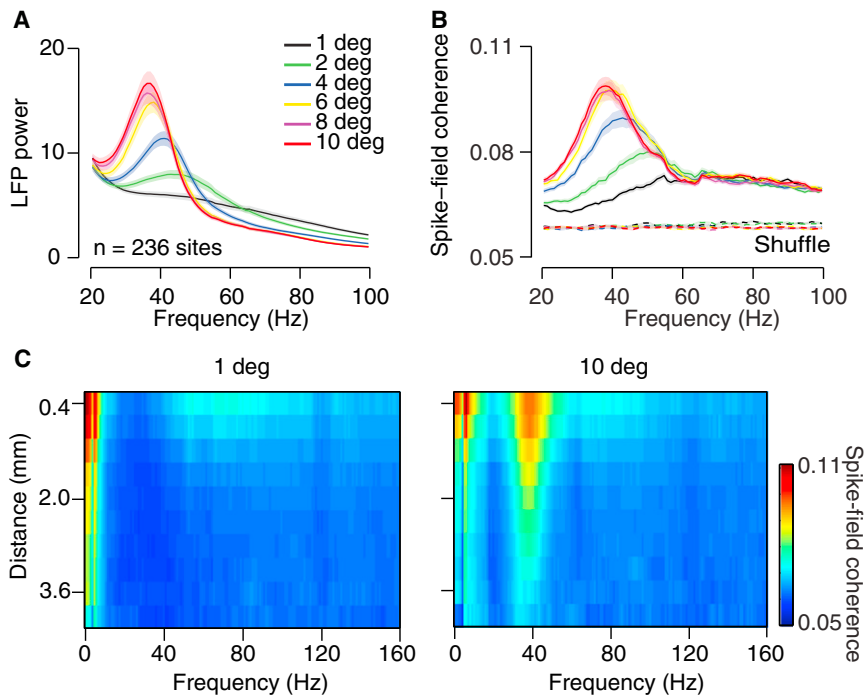


**Figure 1. Effects of Stimulus Size on LFP Gamma Power and SFC**

(A) LFP spectra for responses to gratings ranging from 1 to 10 degrees in diameter. Only higher-frequency components are illustrated for clarity of display. Shading indicates SEM.

(B) Average SFC for gratings of different sizes. Dashed lines indicate the coherence calculated after shuffling the trials. Shading indicates SEM.

(C) SFC as a function of interelectrode distance for 1 and 10 deg gratings ( $n = 10,212$  pairings).

condition. We then averaged responses across all stimulus orientations for all sites, regardless of orientation preference.

Consistent with previous studies, we found that gamma power (30–50 Hz for all analyses) was enhanced and its peak frequency reduced for larger stimuli (Figure 1A;  $n = 236$  sites). Two degree stimuli (green) induced a weak gamma “bump” with a peak frequency of 43 Hz. For 10 degree stimuli (red), the peak frequency shifted to 37 Hz and gamma power increased substantially.

paired our V1 measurements with simultaneous recordings from downstream V2 neurons and found corticocortical coupling was more effective when gamma was elevated.

## RESULTS

### The Relationship between Spike Timing and Gamma Components of the LFP in V1

We used multi-electrode arrays implanted in V1 to record spiking activity and LFPs simultaneously. Electrodes were 1 mm in length and implanted to a nominal depth of 0.6 mm, so that our recordings were primarily from layers 2/3 and 4B, the layers projecting directly to higher cortex. We recorded spiking activity from both single units and multiunits (well-defined waveforms from a handful of cells; see [Experimental Procedures](#)). We observed no significant difference between these signals and pooled their data; separate analysis of single unit responses for the core results are shown in [Figure S1](#) (available online), as indicated below. Visual fields of the recorded units were  $2^\circ$ – $4^\circ$  from the fovea, in the lower visual field.

We measured responses to full contrast drifting gratings ranging in size from 1–10 degrees. Stimulus size affects both gamma power and its peak frequency ([Gieselmann and Thiele, 2008](#); [Jia et al., 2011, 2013](#); [Ray and Maunsell, 2011](#)), making it a useful manipulation for investigating the relationship between spike timing and gamma. Because we studied stimulus-induced gamma, we focused only on sites that were driven by the visual stimulus. So that a common set of sites could be compared across conditions, we analyzed responses only from those sites where neuronal receptive fields were strongly overlapping the smallest stimulus. We presented gratings of 16 different orientations so that all sites would be driven by at least one stimulus

To test whether enhanced gamma power was reflected in a tighter relationship with spike activity, we calculated the spike-field coherence (SFC) for each stimulus size. SFC reflects both amplitude covariation and the phase consistency of two signals, with a value of 0 indicating no relationship and 1 indicating a perfect relationship. We used the LFPs recorded at electrodes adjacent to the one measuring spiking activity, to preclude direct spectral contamination of LFPs by spike waveforms ([Ray and Maunsell, 2011](#)). Because of surround suppression ([Angelucci and Bressloff, 2006](#)), the firing rate for large gratings was on average 51% of that for small gratings. To be sure that this did not influence our measurements, we equated firing rates across conditions by down-sampling responses to match those of the weakest response for all analyses (see [Experimental Procedures](#)).

Gamma-band SFC was 36% higher for activity driven by large (10 degree; [Figure 1B](#), red) gratings compared to small gratings (1 degree; black;  $0.091 \pm 0.002$  versus  $0.067 \pm 0.001$ ,  $p < 0.0001$ ; see [Figure S1](#) for analysis with single units only). This was not the case for the 60–100 Hz frequency range, for which power but not SFC was modulated by stimulus size ([Figure 1A](#)). In addition to an increase in gamma SFC magnitude, we observed a decrease in gamma SFC peak frequency for larger stimuli, from 54 to 36 Hz. The correlation at each site between the peak gamma frequency of LFP power and SFC for stimuli of different sizes was  $0.89 \pm 0.04$  on average. Thus, when LFP gamma power was elevated, there was an enhanced relationship with spiking activity, particularly at the frequency at which gamma power was maximal.

To determine the spatial extent of elevated gamma-band SFC, we compared spikes and LFPs recorded by sites separated by a range of distances ( $n = 10,212$  pairings). Coherence in the gamma band was elevated across several millimeters for activity

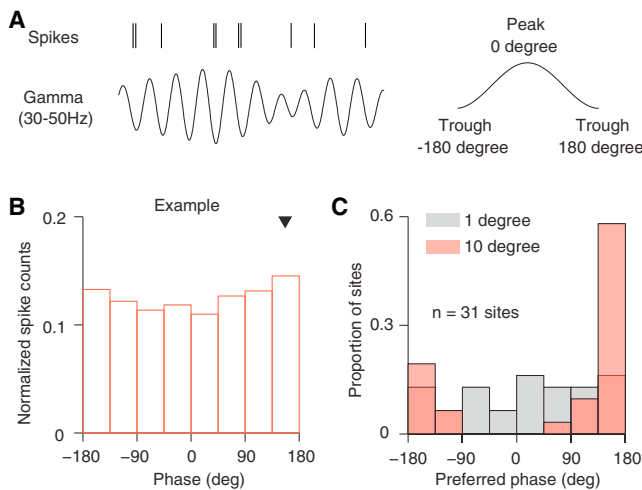


**Figure 2. Gamma Phase Modulation of Spiking Activity**

(A) Illustration of the method.

(B) Spike count distribution within the gamma cycle for an example site. The histogram is normalized to unit area. The preferred phase is indicated with a black triangle. Activity was driven by 10 degree gratings.

(C) Distributions of preferred phase of individual sites from an example array, for activity driven by small (1 deg; gray) and large (10 deg; red) gratings.

driven by 10 degree but not 1 degree gratings (Figure 1C). For the larger grating, gamma coherence decayed from  $0.091 \pm 0.002$  for sites separated by 400 microns to  $0.071 \pm 0.001$  for sites separated by 3.2 mm, a trend that was well described as an exponential decay with a space constant of 2.8 mm. The spatially extensive gamma SFC is consistent with the long-range LFP-LFP coherence in the gamma band, for signals induced by large drifting gratings (Ray and Maunsell, 2010; Jia et al., 2011).

In order to test how enhanced SFC was reflected in the gamma-modulation of spike timing, we measured the distribution of spikes within a gamma cycle for each unit. We band-pass filtered the raw LFP to isolate its gamma components and then applied the Hilbert transform to estimate the phase of this composite signal at each instant (Figure 2A; Montemurro et al., 2008; Colgin et al., 2009; see Experimental Procedures). The distribution of spikes evoked by a 10 degree grating, with respect to gamma phase, is shown for one unit in Figure 2B. There was a slightly higher tendency for spikes to occur at a phase near 180 degrees, corresponding to the trough of the gamma rhythm.

To quantify effects across units, we determined the preferred gamma phase and the phase bias for each neuron or MUA site (see Experimental Procedures). For the example unit (Figure 2B), the preferred phase was 156 degrees (arrowhead) with a bias of 0.46, where a value of 0 indicates no phase modulation and 1 indicates an elevated response at a single phase. Figure 2C shows the distribution of preferred phases for all units in one implant. Neurons had a tendency to fire at the trough of the gamma cycle when activity was driven by 10 degree gratings (red), but not by 1 degree stimuli (gray). Correspondingly, the mean bias in this implant was  $0.37 \pm 0.02$  for activity driven by large gratings, compared to  $0.24 \pm 0.03$  for small ones ( $n = 31$  sites;  $p = 0.0003$  for difference). Across implants, the bias

observed for responses to large gratings ( $0.33 \pm 0.01$ ) was also significantly greater than for small ( $0.25 \pm 0.01$ ;  $p < 0.0001$ ). Further, 25.4% of individual sites ( $n = 236$ ) were significantly gamma modulated when activity was driven by small gratings, but this increased to 54.2% for activity driven by large gratings (Rayleigh test, significance level = 0.05; no correction for multiple comparisons).

In summary, the clustering of spike times in the gamma cycle is more evident when LFP gamma power is more prominent. When driven by large gratings, spikes from individual neurons have a tendency to cluster at the same gamma phase.

### Influence of Gamma on Neuronal Synchrony in V1

Since individual neurons tend to fire at the same phase of a coherent gamma rhythm, the probability that these neurons fire synchronously should be elevated when LFP gamma power is enhanced. The degree to which this occurs will depend on whether neurons tend to fire in the same gamma cycles or in different epochs.

We therefore compared the coordination of pairwise spiking activity in a neuronal population driven by small and large gratings. Because accurate estimation of spike timing correlation requires a large number of spikes, we measured responses to many presentations (300–400) of 10 degree gratings and ones 2–3.5 degrees in size. The smaller size was chosen to cover all of the spatial receptive fields but induced a clearly weaker gamma rhythm than the larger stimulus (Figure 1A). Large and small stimuli were presented in separate blocks of trials, so the number of recorded neurons varied slightly between conditions with this stimulus protocol.

We measured spike timing correlation by calculating cross-correlograms (CCGs) between all neuron pairings. The average shuffle-corrected CCG had a broad peak several hundred milliseconds wide, and a narrow peak (Figure 3A). The broad peak indicates a tendency for the firing of the neurons to cofluctuate on a time scale of a few hundred milliseconds (Smith and Kohn, 2008), whereas the narrow peak indicates a tendency for the neurons to fire synchronously. CCGs had a larger peak at 0 ms time lag for activity evoked by large (Figure 3A; red line;  $n = 51,980$  cell pairs) compared to small gratings (black line;  $n = 53,463$  pairs). The CCG for the former condition also showed clear oscillatory side lobes, indicating rhythmicity in the coordinated firing. This was reflected in the power spectrum of the CCG: gamma power increased strongly, with a shift in peak frequency from 47 Hz to 38 Hz for activity driven by large gratings (Figure 3B). Gamma band spike-spike coherence (a measure of spiking coordination in the frequency domain) was also significantly stronger with a lower peak frequency for activity driven by large gratings (Figure S2).

To isolate synchrony from co-fluctuations over longer time scales, we corrected the raw CCG with a predictor derived from data in which spike times were jittered in a window of 25 ms (see Experimental Procedures). This removes all correlations arising on timescales larger than the jitter window (Smith and Kohn, 2008). Synchrony, measured as the mean amplitude of the jitter-corrected CCG peak ( $\pm 1$  ms of 0 ms time lag), was 2-fold larger for activity driven by large gratings than small ones ( $3.83 \pm 0.06E-4$  versus  $1.92 \pm 0.05E-4$  coin/spk,

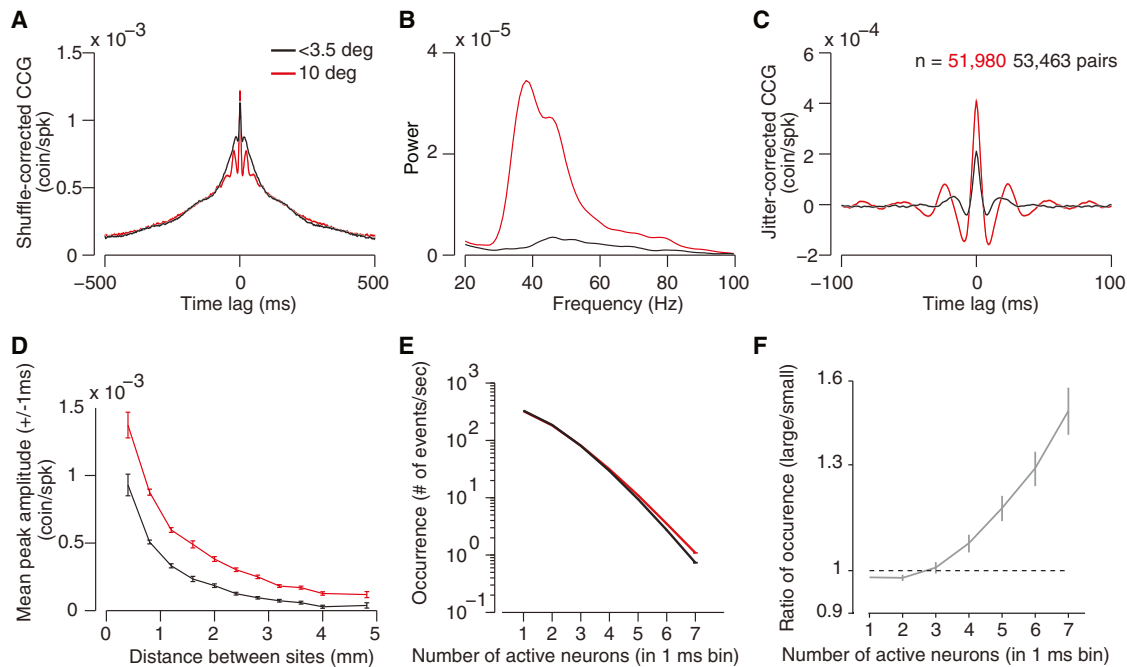


**Figure 3. V1 Neuronal Synchrony**

- (A) Average shuffle-corrected CCGs for large (red) and small (black) gratings. Shading, similar in size to the line thickness, indicates SEM.  
 (B) Power spectra of the CCGs in (A).  
 (C) Average jitter-corrected CCGs for large and small gratings. Shading indicates SEM.  
 (D) Average jitter-corrected CCG peak amplitude, as a function of distance between recording sites. Error bars indicate SEM.  
 (E) Rate of occurrence of different multineuron spiking events ( $n = 990,000$  epochs of 1 ms duration).  
 (F) Ratio between the rates shown in (E). Error bars indicate 95% confidence intervals based on bootstrapping.

$p < 0.0001$ ; Figure 3C; see also Figure S1). The stronger pairwise synchrony in the population involved both nearby and more distant pairs (Figure 3D). Note that the cortical magnification factor for the location of our recordings was roughly 2–3 mm/deg, so synchrony was largely specific to neurons with overlapping spatial receptive fields (Van Essen et al., 1984). Although the increase in synchrony was substantial, synchronous events were rare even when gamma power was elevated.

We extended our analysis beyond pairwise synchrony by calculating the frequency of higher-order synchronous events: that is, events consisting of multiple neurons firing within 1 ms of each other. For activity driven by large gratings (red line), there were more events consisting of several cells firing synchronously, and fewer consisting of either only one neuron firing alone or two neurons firing simultaneously, compared to responses to small gratings (Figures 3E and 3F;  $n = 990,000$  1 ms epochs). Note that events consisting of two neurons firing together (which become less frequent when stimulus size is increased) are not equivalent to measures of pairwise synchrony: the former is defined as *only* two cells in the recorded population firing, whereas measures of pairwise synchrony do not consider activity in a broader population. In complementary analysis, we found that the event-triggered average of the LFP contained more prominent gamma fluctuations, when it was based on higher-order synchronous events (Figure S3).

In summary, the gamma modulation of spike timing in individual neurons is associated with enhanced pairwise and

higher-order synchrony. Increasing stimulus size, which results in more LFP gamma power and a reduction in gamma peak frequency, also enhances population spiking synchrony and causes a shift in that coordination to lower gamma frequencies.

### Coupling of V1 and V2 Spiking Activity

For changes in gamma activity to be indicative of altered cortico-cortical communication, the coordination of spiking activity when gamma is elevated must be sufficient to alter spiking activity in downstream networks. To determine the consequence of the altered coordination of V1 spiking activity, we paired our V1 recordings with simultaneous measurement of V2 activity (Figure 4A).

In the macaque monkey, V2 responses are driven primarily by V1 input. Reversible cooling of V1 results in the near abolition of visually driven responses in V2 (Girard and Bullier, 1989), although some recovery may occur after more permanent lesions (Schmid et al., 2009). Corticocortical projections from V1 originate in layers 2/3 and 4B; fibers projecting to V2 terminate primarily in layer 4 and deep layer 3 (Rockland, 1992). We thus paired our V1 array with an array of tetrodes and electrodes placed near these layers in V2, at a nominal depth of 400–800 microns from the layer 6/white matter border of V2. We made use of the retinotopic organization of these two areas to target V2 neurons having spatial receptive fields aligned with those in V1 (Figure 4B). We recorded at 8 sets of V2 sites (up to 7 tetrodes per set) in 5 animals, providing 220 V2 neurons.

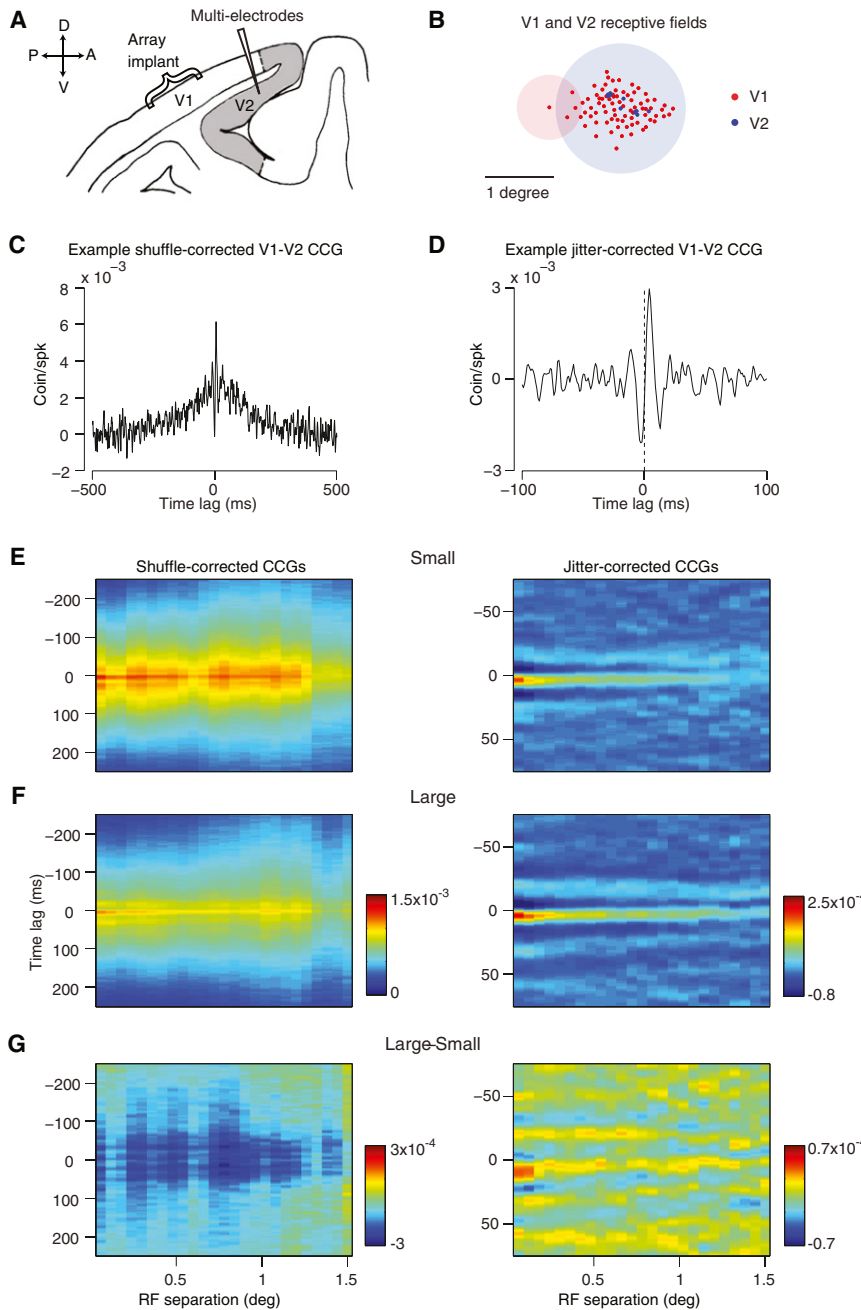


**Figure 4. Relating Spiking Activity in V1 and V2**

(A) Illustration of the experimental approach. (B) Centers of the spatial receptive fields (RFs) in V1 (red) and V2 (blue). Each dot indicates the RF center at a single site. The large circles indicate the extent of an exemplar V1 and V2 RF. (C) Example of shuffle-corrected V1-V2 CCG from one pair for large gratings. (D) Jitter-corrected CCGs (jitter window = 25 ms) for the pair in (C). (E and F) Average shuffle-corrected (left) and jitter-corrected (right) V1-V2 CCGs as a function of RF separation (distance between centers) for small (E;  $< 3.5\text{ deg}$ ) and large (F;  $10\text{ deg}$ ) gratings. (G) For shuffle-corrected (left) and jitter-corrected (right) V1-V2 CCGs, the difference between CCGs of responses to large and small gratings. Color bars indicate CCG values in coin/spk.

layers: V1-V2 CCGs often included a broad peak, but narrow peaks were observed only at depths consistent with the expected termination site of V1 fibers (Smith et al., 2012).

We measured how V1-V2 CCGs differed for activity driven by large and small gratings, as a function of the RF separation between V1 and V2 recording sites (center-to-center spacing). Narrow and broad CCG peaks were larger at more overlapping locations for both small and large grating, but there were several differences between these conditions. First, the average shuffle-corrected V1-V2 CCG for responses to large gratings ( $n = 21,993$  pairs; Figure 4F, left) showed a suppressed broad component compared to those from responses to small gratings ( $n = 22,367$  pairs; Figure 4E, left). This is made apparent by subtracting the CCGs for activity driven by small gratings from those for large gratings (Figure 4G, left). We note that the suppression of the broad peak was accompanied by a loss of low-frequency power in the

We determined the strength of corticocortical coupling by measuring the relationship of V1 spiking activity with that in V2. An example shuffle-corrected CCG of one V1-V2 pair driven by large gratings shows a broad peak, corresponding to slow time-scale correlation between V1 and V2 neurons, with a superimposed narrow peak (Figure 4C). The jitter-corrected CCG (25 ms jitter window) of the pair has a clear positive peak (Figure 4D) offset from 0 ms time lag, indicating that the V2 neuron had a higher probability to fire 3 ms after a spike in the V1 neuron. This is consistent with the conduction and synaptic delays for signals between these areas (Girard et al., 2001). In separate experiments, we sampled responses systematically across V2

LFP (Figure S4); a similar but weaker effect was evident in V1-V1 CCGs (Figure 3). Second, gamma power in the shuffle-corrected V1-V2 CCG increased roughly 1.5 fold for the larger stimulus, and gamma peak frequency decreased from 43 to 40 Hz (visible in Figures 4E-4G, right).

While the broad peak was suppressed, jitter-corrected CCGs for responses to large gratings showed an enhanced sharp peak. For pairs whose receptive fields were separated by less than 1 degree, the average jitter-corrected CCG showed a 28% increase in mean amplitude for activity driven by large ( $n = 15,919$  pairs) compared to small gratings ( $n = 16,061$  pairs;  $1.38 \pm 0.06 \times 10^{-4}$  versus  $1.07 \pm 0.06 \times 10^{-4}$  coin/spk;  $p < 0.001$ ; see

also Figure S1), indicating stronger V1-V2 coupling when gamma power was elevated. In 1.7% of individual V1-V2 pairs ( $n = 272$  pairs) the jitter-corrected CCG peak was significant (see [Experimental Procedures](#)), with a mean peak offset of  $2.7 \pm 0.2$  ms. In these pairs, we observed a 92% enhancement in average CCG amplitude ( $p = 0.02$ ) compared to responses driven by small gratings. Importantly, the modulation of V1-V2 CCGs by stimulus size was retinotopically specific. For pairs with a greater RF offset, sharp CCG peaks were rarely observed and the mean CCG area increased by only 11%, from  $0.63 \pm 0.01E-4$  ( $n = 6,306$ ) to  $0.70 \pm 0.10E-4$  coin/spk ( $n = 6,074$ ;  $p = 0.62$ ) for responses to small compared to large gratings. In complementary analysis, we found that V1-V2 coupling was stronger for events that consisted of several V1 neurons firing at the same time (Figure S3), which became more frequent when gamma power was elevated (Figures 3E and 3F).

We conclude that stimuli that induce stronger gamma power also result in an enhancement of brief timescale coupling of V1-V2 spiking activity. This effect was stronger in the small percentage (1.7%) of V1-V2 pairs that had significant CCGs and thus the clearest functional interaction. A weaker enhancement was seen in pairs with retinotopically aligned receptive fields, and no effect was seen for those pairs with offset receptive fields.

### The Role of V1 and V2 Gamma Rhythms in Modulating Coupling

The stronger V1-V2 coupling for spiking responses that are more gamma-modulated could arise from two distinct mechanisms. First, each V1 spike was more likely to be accompanied by synchronous spikes in the V1 population when gamma was elevated (Figure 3). A V2 cell integrating these inputs would thus be more likely to fire, causing a larger peak in V1-V2 CCGs at short time lags. Alternatively, coupling may be enhanced because V1 input arrives at the V2 gamma phase at which V2 neurons are most likely to fire. We next aimed to determine whether V1 and V2 gamma rhythms were coordinated, and how these two rhythms influence the coupling of V1-V2 spiking activity.

We first measured the coherence between V1 and V2 LFPs, as a function of the separation between the spatial RFs of neurons recorded at each site (Figure 5A). Coherence was stronger between sites representing similar visual locations. Large gratings, which induce more gamma power both in V1 (Figure 1) and V2 (Figure S5), resulted in stronger gamma band coherence and a shift to lower frequencies. Between sites with receptive fields separated by less than 1 degree, gamma band coherence was  $0.424 \pm 0.002$  for activity driven by large gratings, compared to  $0.377 \pm 0.001$  for small gratings ( $p < 0.0001$ ;  $n = 2,197$  pairs of sites; Figure 5B). This elevation of LFP coherence for larger gratings was also accompanied by enhanced gamma band coherence between V1 spikes and V2 LFP coherence (Figure S2) as well as higher-order V1 events and the V2 LFP (Figure S3).

We then used coherence analysis to measure the phase difference between the V1 and V2 gamma rhythms. For activity induced by large gratings, when gamma was most prominent, the circular mean phase difference was  $88.0 \pm 0.3$  degrees (Figure 6A). This corresponds to a delay of 5–8 ms between the two

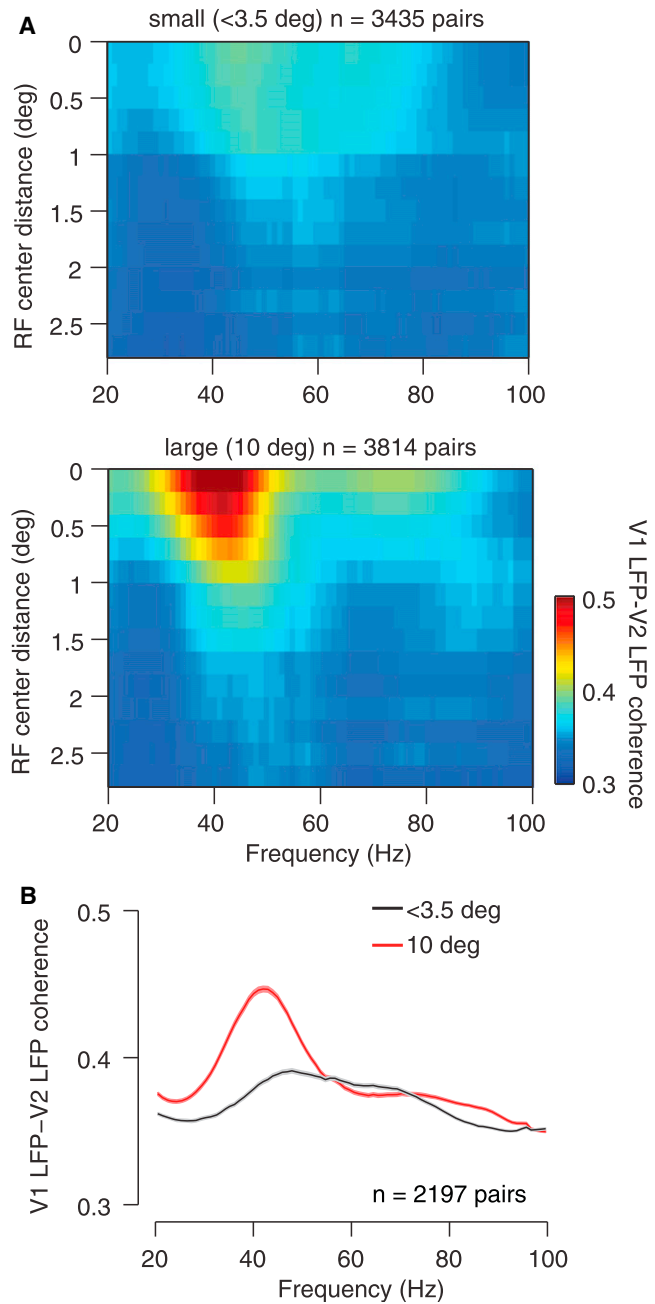


**Figure 5. Coherence between V1 and V2 LFPs**

(A) Coherence as a function of frequency and V1-V2 RF separation for responses to small (top) and large (bottom) gratings. There were too few recording sites separated by 1.5–2.8 degrees to measure spiking correlation (Figure 4) accurately, but these limited data provided consistent measurements of field-field coherence and are shown here.

(B) Average coherence as a function of frequency, for sites for which RFs were separated by less than 1 degree. Shading indicates SEM.

rhythms (for to a gamma period of 20–33 ms, or 30–50 Hz). Note that this is larger than the 2.7 ms delay between V1 spiking activity and that in V2, indicated by V1-V2 CCGs. The V1-V2 phase offset is also higher than the relative phase of gamma

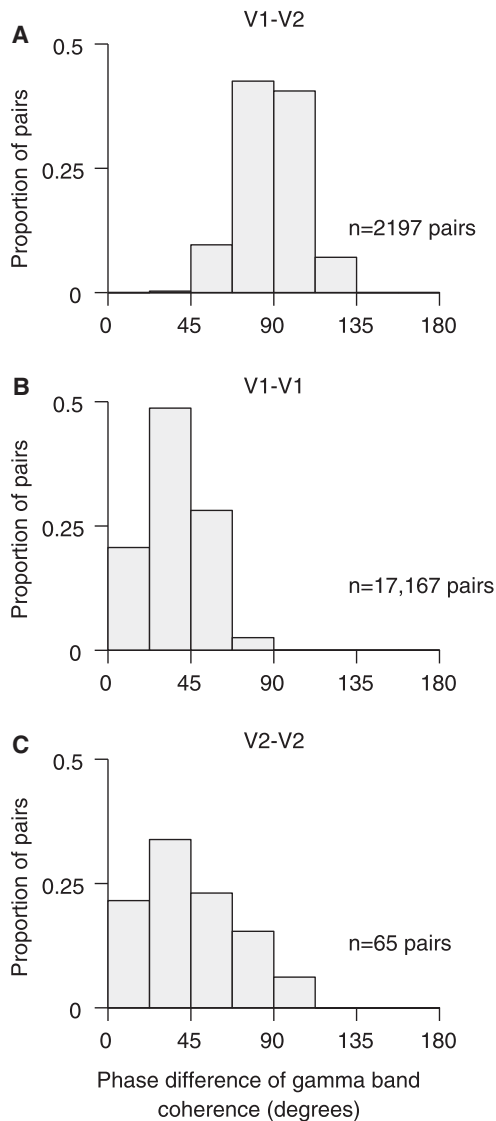


**Figure 6. Phase Difference in the Gamma Band within and between Cortical Regions**

- (A) Phase difference between V1 and V2 gamma rhythms for sites with RFs separated by less than 1 degree.  
 (B) Phase difference in the gamma band between pairs of V1 sites, for the same V1 sites as in (A).  
 (C) Phase difference in the gamma band between pairs of V2 sites, for the same V2 sites as in (A).

rhythms recorded within each cortical area from the same sites:  $36.9 \pm 0.1$  degrees for V1 sites (Figure 6B;  $p < 0.0001$  for difference with V1-V2 phase distribution based on bootstrap analysis) and  $46.2 \pm 3.2$  degrees for V2 sites (Figure 6C;  $p < 0.0001$ ).

We next determined whether the change in V1-V2 coupling was due to V1 input arriving at the preferred phase of V2 gamma, or whether altered coordination of V1 spike timing was primarily responsible. We used responses to large gratings and determined the phase of spikes relative to the gamma cycle, as in Figure 2 (Figure 7A, red). We normalized the phase distribution for

each cell to unit area and then averaged across all cells. We defined the preferred V1 gamma phase ( $\phi$ ) for each implant as the phase at which the probability of V1 spikes was maximal. Consistent with Figure 2, population V1 spiking activity was gamma modulated (Figure 7B; ANOVA,  $F = 285$ ,  $p < 0.0001$ ). For each phase and V1-V2 pairing, we then calculated the proportion of V1 spikes that were followed by a spike in V2 0.5–3.5 ms later, a window that reflects the offset of the narrow V1-V2 CCG peak ( $\sim 2.5$  ms). The proportion was significantly modulated by V1 gamma phase (ANOVA,  $F = 3.81$ ,  $p = 4E-4$ ) and highest at the gamma phase at which V1 spiking was maximal (Figure 7C). This is consistent with enhanced V1-V2 coupling arising at least in part from the temporal coordination of V1 spiking.

To test the influence of the V2 gamma rhythm, we determined the V2 preferred gamma phase, defined as the phase at which V2 cells were most likely to fire. V2 firing was less strongly gamma-modulated than in V1 (Figure 7D, solid line), but the modulation was statistically significant ( $F = 8.98$ ,  $p < 0.0001$ ). We then computed the proportion of V1 spikes that were followed by a V2 spike, based on their timing with respect to V2 gamma phase (Figure 7F). If V2 gamma phase strongly modulated the efficacy of V1 input, this proportion should peak  $\sim 2.5$  ms ( $\sim 30$  deg) before the V2 preferred phase. However, modulation was weak and not significant ( $F = 1.14$ ,  $p = 0.34$ ). Further, there was a tendency for coupling to be slightly higher at phases roughly 90 degrees earlier than the V2 preferred phase. This is similar to the phase offset between V1 and V2 gamma (Figure 6) and suggests that the coupling of V1-V2 spiking activity follows more closely the V1 than the V2 gamma rhythm. To confirm this, we calculated the phase distribution of V1 spikes with respect to V2 gamma. This revealed a significant modulation of V1 firing ( $F = 65.2$ ,  $p < 0.0001$ ) that was offset by 90 degrees from the preferred phase of V2 spiking (Figure 7E, solid line).

We were concerned that the weaker modulation of spike timing by V2 gamma might influence our results. We therefore analyzed the responses of a subset of V2 neurons ( $n = 38$  cells) whose firing was more strongly modulated, meaning that these cells had a phase bias larger than 0.4 (as defined in Figure 2). These neurons, by definition, were well-modulated by V2 gamma (ANOVA,  $F = 10.35$ ,  $p < 0.0001$ ; Figure 7D, dashed line). As for the larger population, V1-V2 coupling was strongest at a V2 gamma phase 90 degrees earlier than that at which V2 neurons were most likely to fire (Figure 7F, dashed line). This peak occurred at a phase at which the simultaneously recorded V1 spikes ( $n = 306$  cells) tended to occur ( $F = 167$ ,  $p < 0.0001$ ; Figure 7E, dashed line).

Together, our results suggest that a V1 spike is more likely to be followed by a V2 spike when the V1 cell fires at the V1 preferred gamma phase. This is consistent with enhanced V1-V2 coupling arising from the coordination of the V1 population response. In contrast, V1 spikes are not most likely to be followed by a V2 spike when they occur just (i.e.,  $\sim 2.5$  ms) before the V2 gamma phase at which V2 cells are most likely to fire. This can be attributed to a roughly 90 degree phase shift between the gamma rhythms in these two areas, longer than the delay for spike propagation between these networks (2.7 ms, on average). Thus, gamma-modulated V1 activity tends

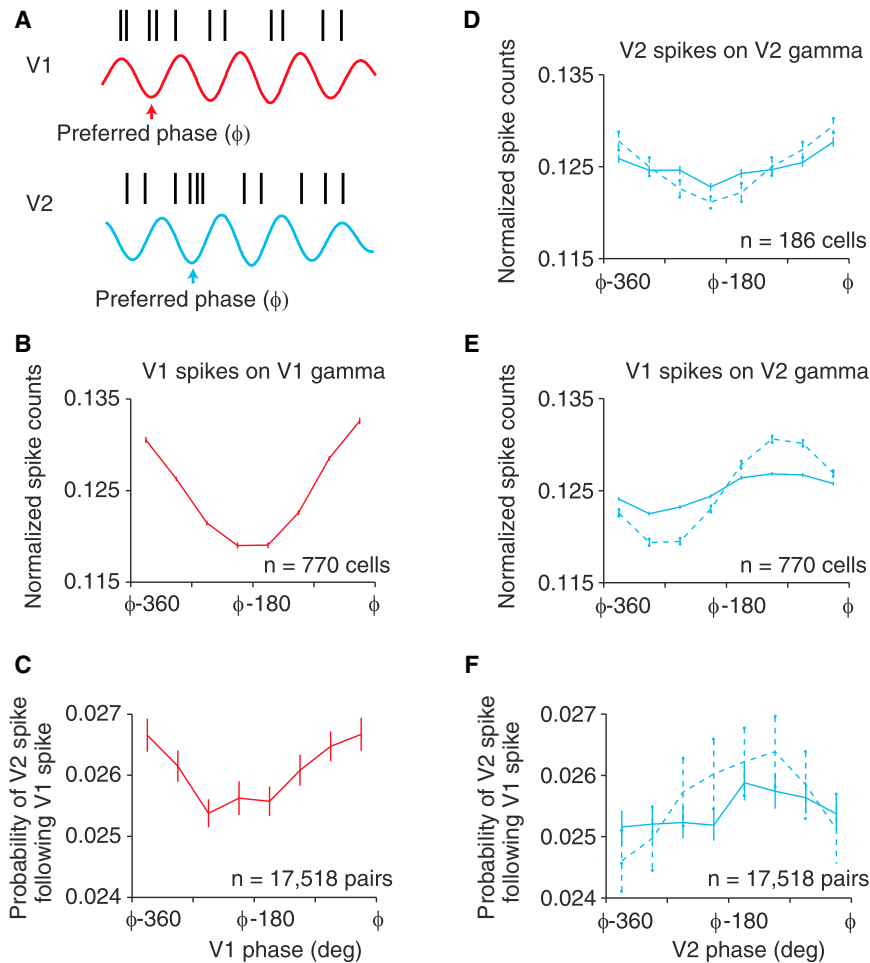


**Figure 7. Coupling of V1 and V2 Spiking Activity, Relative to the V1 and V2 Gamma Rhythms**

(A) The preferred gamma phase ( $\phi$ ) was defined as the phase at which local V1/V2 spiking activity was most likely. (B) V1 spike counts relative to the V1 gamma cycle, with the preferred phase plotted as the last bin. (C) Proportion of V1 spikes followed by a V2 spike 1–3 ms later, for each V1 gamma phase. (D) Normalized V2 spike counts relative to the V2 gamma cycle (solid line: all  $n = 186$  cells; dashed line: 38 neurons with phase bias  $> 0.4$ ). (E) Normalized V1 spike counts aligned with respect to the V2 gamma phase at which V2 firing is most likely (solid line: all  $n = 770$  cells; dashed line: 306 neurons recorded simultaneously with the V2 neurons with a phase bias  $> 0.4$ ). (F) Proportion of V1 spikes that are followed by a V2 spike, with respect to the V2 gamma phase (solid line: all  $n = 17,518$  pairs; dashed line:  $n = 2,117$  pairings with V2 neurons with a bias  $> 0.4$ ). Error bars indicate SEM.

to arrive in V2 several milliseconds before the optimal V2 gamma phase.

#### Orientation Dependence of the Spike-Gamma Relationship

In addition to enhancing gamma power, increasing stimulus size suppresses the firing of many V1 neurons (Angelucci and Bressloff, 2006), an effect that may involve an alteration in the balance of cortical excitation and inhibition (Haider et al., 2010). Larger stimuli also recruit activity in a more spatially distributed network. These effects complicate the interpretation of size-dependent changes in gamma and the coordination of spiking activity.

We therefore carried out three additional analyses. First, we divided the trials for responses to large gratings based on gamma power. If there is a consistent relationship between gamma and the coordination of spiking activity, then trials with more gamma power should have more synchrony and tighter coupling to V2 cells. V1 synchrony and V1-V2 coupling were significantly higher on trials with more gamma (Figure S6). Second, we found variations in LFP gamma power across animals and this was predictive, on an animal-by-animal basis, of the change in the coordination of V1 spiking and V1-V2 coupling (Figure S7).

Finally, we compared responses to stimuli of different orientations but of a fixed size. The gamma induced by large gratings has a common orientation preference across recording sites within several millimeters of each other (Berens et al., 2008; Jia et al., 2011). This is illustrated in Figure 8A, which shows the tuning of gamma power averaged across sites from the same implant. In this example, gratings with an orientation of 112.5 degrees (red circle) induced 2.7-fold more power than gratings oriented at 45 degrees (gray circle). The orientation that induced more power also led to a more coherent gamma rhythm across sites (Figure 8B; top), with a smaller range of phase delays (bottom). Across stimulus orientations, gamma power and coherence were significantly correlated ( $r = 0.89 \pm 0.02$ ,  $n = 8$  implants). Firing rates, however, were similar for the orientations inducing the most and least gamma power ( $9.17 \pm 0.35$  versus  $9.31 \pm 0.36$  sp/s, respectively;  $n = 957$  neurons;  $p = 0.7$ ).

To test whether the orientation-dependent changes in gamma power and coherence were associated with altered coordination of V1 spiking activity, we compared jitter-corrected V1-V1 CCGs for the stimulus orientations that induced the most (Figure 8C, red) and least (black) gamma power. The orientation that generated higher gamma power resulted in 74% stronger population synchrony in V1 ( $5.8 \pm 0.1E-4$  versus  $3.4 \pm 0.1E-4$  coin/spk;  $p < 0.0001$ ).

We then compared V1 and V2 spiking activity for these two stimulus conditions for cell pairs whose receptive fields were separated by less than one degree. We first confirmed that the orientation that induced the strongest gamma power in V1 also did so in V2 (Figure S5). We then computed jitter-corrected V1-V2 CCGs and found these showed an 85% enhancement of

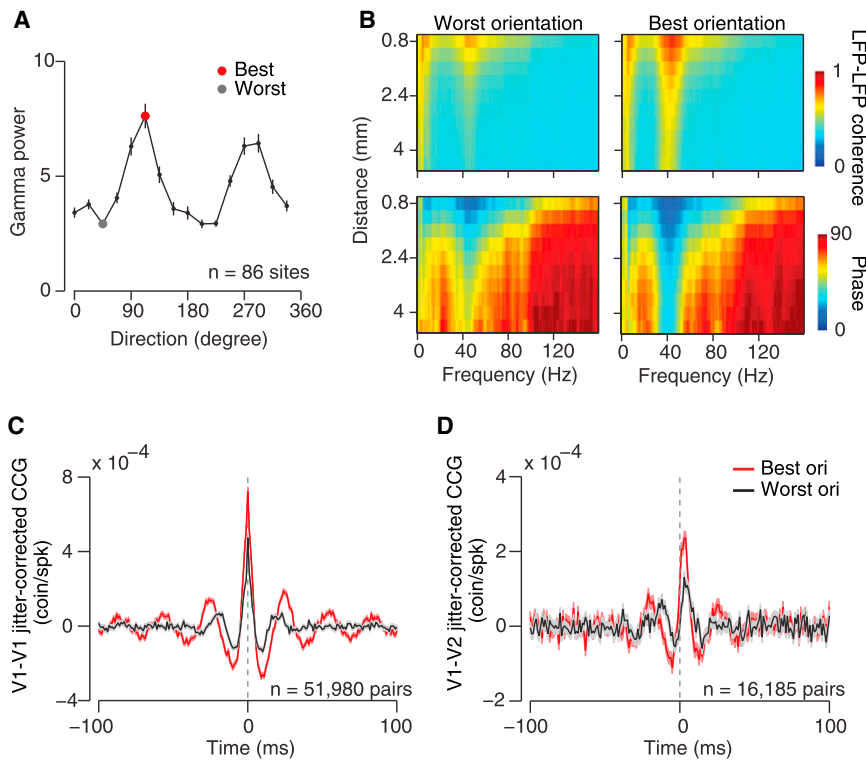


**Figure 8. Dependence of LFP Gamma Power and Neuronal Coordination on Stimulus Orientation**

(A) Population orientation tuning of gamma power from one example array, for activity induced with large gratings. The red dot indicates the orientation that induced the most power; the gray dot indicates the worst orientation.

(B) Coherence and phase difference between LFPs in V1, as a function of interelectrode distance and frequency ( $n = 2,961$  pairs).

(C) Averaged jitter-corrected V1-V1 CCGs for the best and worst stimulus orientations. The data shown are those of Figure 3, but not restricted to sites driven by small gratings.

(D) Averaged jitter-corrected V1-V2 CCGs for the best and worst stimulus orientations.

Error bars (A) and shading (C and D) indicate SEM.

peak amplitude for the orientation that induced the most gamma, compared to that inducing the least (Figure 8D;  $2.1 \pm 0.1E-4$  versus  $1.1 \pm 0.1E-4$  coin/spk;  $p < 0.0001$ ). This was also apparent in the gamma band V1 spike-V2 LFP coherence (Figure S2).

We conclude that the relationship among gamma power, V1 population synchrony and coupling of V1-V2 spiking activity does not depend on changes in stimulus size. Manipulations of stimulus orientation reveal similar effects.

## DISCUSSION

We examined the relationship between the gamma components of the LFP and spike timing in a distributed neuronal population, and tested the influence of coordinated ensemble activity on corticocortical signaling. We found that visual stimuli that induce a strong, coherent gamma rhythm in V1 also result in spiking activity that is more strongly gamma phase modulated and in enhanced V1 pairwise and higher-order synchrony. Under these conditions, there was a higher probability that a V1 spike would be followed several milliseconds later by one in V2. This effect was retinotopically specific, and reflected more closely the gamma rhythm in the upstream (V1) than downstream (V2) area. Changes in gamma power are thus correlated with changes in spike timing of a neuronal population and this can affect coupling between cortical areas.

### Gamma Generation

The LFP reflects summed synaptic and spiking activity in a region surrounding the recording site. The gamma components of the LFP are thought to involve rhythmic inhibition, either due to inhib-

itory network activity or to excitatory-inhibitory neuron interactions (Whittington et al., 2011). Both explanations of gamma generation predict a stronger modulation of spike timing when gamma is elevated, and could thus explain our observations. Both explanations also suggest that excitatory and inhibitory cells fire at different phases of the gamma

cycle. Although we did not distinguish between these cell types in our extracellular recordings, this is unlikely to have caused an underestimate of gamma modulation of spike timing because inhibition and excitation are only offset by a fraction of a gamma cycle (Atallah and Scanziani, 2009; Hasenstaub et al., 2005).

Our results show that elevated LFP gamma power is a useful marker of spike timing coordination. They do not indicate that gamma causes this coordination. Indeed, since gamma reflects rhythmic inhibition, which in turn modulates spike timing, it is difficult to define whether enhanced gamma leads to stronger coordination of activity or vice-versa—the two are inextricable. Gamma components of the LFP could only actively coordinate activity through ephaptic effects. Such effects are weak for low amplitude, high frequency cortical rhythms but may have a measurable effect on neuronal populations (Fröhlich and McCormick, 2010).

### Gamma and Neuronal Synchrony

Previous measurements of gamma modulation of neuronal spiking activity and of pairwise synchrony have provided positive and negative evidence (see Gray, 1999, for review). This may be because gamma fluctuations can be difficult to detect, as they vary in frequency, are transient, and are not stimulus locked (see Friedman-Hill et al., 2000). LFP gamma power has been suggested as a more sensitive measure (Gray and Singer, 1989; Zeitler et al., 2006), but its relationship to spike timing in a distributed neuronal ensemble has remained unclear.

Previous attempts to relate enhanced LFP gamma power to changes in spiking activity have relied primarily on measuring

the LFP-spiking relationship (Fries et al., 1997, 2001; Gregoriou et al., 2009; Fries et al., 2008; Colgin et al., 2009). This has shown that enhanced LFP gamma power is paralleled by an increase in gamma SFC and gamma modulation of single neuron spike trains, as in our Figures 1 and 2. Few studies have attempted to relate these observations to changes in spike timing among pairs or larger populations of neurons. Enhanced LFP gamma power is correlated with greater spike-spike coherence (SSC) in the gamma frequencies (Womelsdorf et al., 2007; Fries et al., 2008; Lima et al., 2010), but because gamma represents a small fraction of LFP power the functional importance of this is unclear. Indeed, enhanced gamma SFC and SSC need not be evident by an increase in pairwise spike timing correlation (CCGs; Fries et al., 2008) and gamma-modulation of V1 neuron spiking activity is only weakly correlated with the strength of pairwise synchrony (Samonds and Bonds, 2005).

We induced strong, spatially coherent LFP gamma power and used the power of multielectrode recordings to show that elevated LFP gamma is associated with enhanced pairwise and higher-order synchrony. Further, the peak frequency of gamma-modulated spiking activity shifted toward lower frequencies (38–40 Hz) for large gratings, as did LFP peak gamma power (37 Hz). Peak frequencies for activity driven with small gratings were consistently higher, but varied over a wider range (43–54 Hz). This was due in part to their weak power, making the peak frequency more difficult to measure precisely.

The differences in gamma-modulation of spiking activity we report cannot be ascribed to differences in firing rate. We equated rates across conditions to be sure there would be no statistical issues based on different numbers of spikes for different stimuli. Further, for manipulations of stimulus size, correlations were strongest when rates were lowest, precisely when correlations are most likely to be underestimated (Cohen and Kohn, 2011). We also showed that manipulating gamma by changing stimulus orientation had similar effects to changing size, but caused no obvious difference in population firing rate. It is possible that firing in a broader pool of neurons was higher for the orientation that induced the strongest gamma (Jia et al., 2011). If so, it would only strengthen our argument, as it would indicate stronger gamma modulation both for stimulus manipulations that lower rates (larger stimuli) and increase them (gamma-preferred orientation). Finally, spiking activity was more coordinated on those trials with more gamma power, when no differences in rate were apparent.

### Corticocortical Coupling

Gamma can be coherent between different cortical areas (Buschman and Miller, 2007; Gregoriou et al., 2009) and hippocampal networks (Montgomery and Buzsáki, 2007; Colgin et al., 2009). When this is the case, the spiking activity in one area can be coherent with the gamma components of the LFP recorded in another (Colgin et al., 2009; Gregoriou et al., 2009). This has been taken as evidence that elevated LFP gamma power indicates enhanced communication between neuronal groups, but precisely how spiking activity is coordinated between networks has remained unclear. Our measurements of spiking activity in V1 and V2 showed directly that when gamma power is elevated there is enhanced spike-spike corre-

lation on brief timescales for subsets of neurons with aligned spatial RFs (Figure 4 and 8). This relationship is also apparent in the gamma frequency range of V1-V2 LFP coherence and SFC.

Previous interareal studies of spiking activity have shown correlated oscillatory firing among the retina, LGN, and cortical areas 17 and 18 (Castelo-Branco et al., 1998), but some of this was in higher frequencies bands and it was not retinotopically specific. Engel et al. (1991) performed cross-correlation analysis between neurons in areas 17 and PMLS of the cat, and showed that these could display synchronous rhythmic activity in a retinotopically specific manner. However, the phase in area 17 lagged that in PMLS by 2 ms, suggesting that this involved another pathway than the feedforward projection from area 17 to PMLS (Engel et al., 1991).

Our results extend these observations in several important ways. First, we link measurements of interareal spiking correlations to changes in LFP gamma power and peak frequency. Second, we recorded from networks whose connectivity is well defined, and observed interactions consistent with the propagation delays between them. Finally, we investigated the relative influence of the V1 and V2 gamma rhythms on V1-V2 coupling, providing the first test of how local gamma signals relate to corticocortical signaling of spiking activity.

The enhanced coupling of V1-V2 spiking activity could arise from more synchronous V1 input, or from timing those inputs to arrive when downstream V2 inhibition is at its weakest gamma phase. We therefore compared the probability that a V1 spike would be followed by one in V2, based on timing relative to the V1 and V2 gamma cycles. Determining LFP phase is notoriously difficult (Nelson et al., 2008), so we used the local spiking activity to establish the preferred gamma phase in each area. We found that coupling follows the V1 gamma rhythm more closely than the V2 rhythm. This implies that the coordination of synaptic input modulates interareal coupling more strongly than the regulation of inhibition in the target network. Further, it suggests that downstream gamma rhythms do not strongly gate inputs, as suggested by the coherence-through-communication hypothesis (Fries, 2009), at least for the stimulus-induced gamma that we studied.

The gamma rhythms in V1 and V2 are offset by roughly 90 degrees or ~5–8.3 ms (but see Fries et al., 1994). Since the delay in correlated spiking activity in these two networks is only ~2.5 ms, V1 inputs do not arrive at the optimal V2 gamma phase. The additional gamma phase delay likely reflects the recruitment of V2 circuits that generate gamma in that area. Timing inputs to arrive at a nonoptimal phase of the local rhythm may be necessary to prevent an accumulation of synchrony as signals are passed sequentially through feedforward networks (Reyes, 2003). Our results differ in this regard from those of Gregoriou et al. (2009) who found a difference between the gamma rhythms in frontal eye field and area V4 of 8–13 ms. This was attributed to conduction delays but the coordination of spiking activity in these two areas was not reported in detail.

### The Function of Gamma

We performed our recordings in anesthetized animals. To confirm that the relationship between this signal and spiking

activity was similar in awake animals, we recorded from small populations of V1 neurons in one awake monkey and observed similar effects (Figure S8). Further, the properties of LFP gamma we observed are similar to those previously reported in awake fixating animals (see Figure S8 for more discussion). Thus, it seems unlikely that our results were strongly influenced by anesthesia. However, we cannot rule out the possibility that the gamma induced by attentive processing has properties different from the stimulus-induced gamma that we studied (see also below).

We emphasize that the gamma we studied was stimulus induced. This form of gamma has been suggested to play a role in stimulus binding (Gray, 1999), by coordinating the activity within a distributed representation to enhance its effect on downstream neurons. Our results provide the first direct evidence that such coordination does alter the efficacy of drive to downstream networks. Does this indicate that stimulus-induced gamma modulation is central to visual processing? We believe this is unlikely. First, when gamma power is strongest, the rhythm is coherent across millimeters of cortex (Jia et al., 2011). It may thus lack the specificity needed to select specific subgroups of neurons to be bound or preferentially routed to downstream targets. Second, the dynamics of induced gamma are relatively slow (Jia et al., 2011), peaking 200–300 ms after stimulus onset, at least for grating stimuli. Because visual input changes frequently, these dynamics may limit its functional role, although it remains possible that saccade-related oscillatory activity could coordinate activity near response onset (Ito et al., 2011). Third, gamma power is easily disrupted by discontinuities in visual input (Lima et al., 2010; Ray and Maunsell, 2010; Jia et al., 2011) and the gamma power induced by naturalistic input appears substantially weaker than that induced by grating stimuli (Kayser et al., 2003).

The proposal that gamma plays a further role in corticocortical signaling—communication through coherence (CTC; Fries, 2009)—by gating inputs to downstream networks is not supported by our data. This proposal has typically been studied using the allocation of attention to induce gamma, which was not recruited in our experiments. It is possible that this form of “top-down” gamma has different properties from the “bottom-up” gamma we recorded, or a different ability to gate inputs. However, our stimulus manipulations involved a 2-fold change in gamma power, whereas attentional modulation typically alters gamma by roughly 20%. The change in coordinated spiking activity we observed thus likely represents an upper bound on the physiological range over which gamma fluctuates in vivo, although we cannot exclude the possibility that gamma driven by the allocation of attention has more powerful gating properties despite its weaker power.

More generally, gamma modulation of spiking activity represents but one form of spiking coordination. Numerous cognitive and behavioral factors (e.g., training, learning, arousal, and attention) can influence the coordination of spiking activity (see Kohn et al., 2009 for review), over a range of spatial and temporal scales. Our results provide the first demonstration that such changes in the coordination of activity in one cortical network can have meaningful consequences on coupling to downstream networks (see Bruno and Sakmann, 2006, for related findings in

the thalamocortical circuit). In our case, a manipulation that doubles the strength of pairwise V1 synchrony causes each V1 spike to be roughly twice as likely to be followed by a spike in V2, a dynamic change in functional connectivity similar in magnitude to changes associated with more long-term synaptic modification.

## EXPERIMENTAL PROCEDURES

We recorded from seven adult male macaque monkeys (*M. fascicularis*). Anesthesia was induced with ketamine (10 mg/kg) and maintained with isoflurane (1.5%–2.5% in 95% O<sub>2</sub>) during surgery. Anesthesia during recordings was provided by infusion of sufentanil citrate (6–18 μg/kg/hr, adjusted as needed for each animal). Vecuronium bromide (0.15 mg/kg/hr) was used to suppress eye movements. Physiological signs were monitored to ensure adequate anesthesia and animal well-being. An antibiotic (Baytril, 2.5 mg/kg) and an anti-inflammatory steroid (dexamethasone, 1 mg/kg) were administered daily. All procedures were approved by the IACUC of the Albert Einstein College of Medicine.

We recorded signals using a 100 multielectrode array (10 × 10 grid with 0.4 mm spacing). Although the method of insertion made precise control difficult, the length of the electrodes and their partial insertion into cortex ensured that primarily superficial layers were recorded. The signal on each electrode was filtered between 250 Hz and 7.5 kHz to provide spiking activity. Events that exceeded a user-defined threshold were sampled at 30 kHz and saved for offline sorting. Raw signals were also filtered from 0.3–250 Hz and sampled at 1 kHz to provide LFPs. To record V2 responses, we used up to 7 independent electrodes and tetrodes (305 micron spacing; Thomas Recording). Raw signals recorded were filtered from 0.5–200 Hz for LFPs (digitized at 1 kHz) and 0.5–10 kHz for spiking activity (sampled at 40 kHz).

To remove 60 Hz noise, we applied a fourth order Butterworth band-stop filter to the LFP. Spikes were sorted using commercial software (Offline Sorter) and standard algorithms and criteria. Only units with a waveform signal-to-noise ratio (Smith and Kohn, 2008) larger than 2, corresponding to single units and small clusters of such cells (MUA), were used for further analysis. Our results were not sensitive to the waveform quality threshold.

Stimuli were generated with custom software and presented on a calibrated CRT monitor (1,024 × 768 pixels; refresh 100 Hz) placed 110 cm from the animal. We mapped the RFs in V1 and V2 by briefly presenting small, full contrast drifting gratings (0.6 degree; 250 ms) of different orientations at a range of spatial positions. The spiking responses at each site were fit with a 2D Gaussian to determine the location and extent of the spatial receptive fields. We then centered full contrast gratings (1 cpd, drifting at 6.25 cycles/s) on the aggregate RF.

We used two sets of stimuli. The first contained gratings drifting in 16 different directions (22.5 deg. steps), with diameters ranging from 1–10 degrees. Each stimulus was presented for 1 s in pseudorandomized order (30 repetitions). These stimuli were viewed monocularly (n = 6 implants). The second set used only small (2–3.5 degree) and large (10 degree) gratings of 8 orientations, but each was presented 300–400 times (1.28 s with 1.5 interstimulus interval) to provide sufficient spikes to investigate timing relationships in detail (n = 6 implants). These stimuli were viewed binocularly.

We analyzed response epochs when gamma was prominent and firing rates were relatively stationary, namely 100 ms after stimulus onset until the end of the stimulus presentation. For all comparisons involving stimuli of different sizes, we included only recording sites whose receptive field center was within the radius of the smallest grating.

We analyzed the power spectrum of the LFP and spiking activity with the multitaper method, using the Chronux Toolbox. We applied  $k = 2WT - 1$  orthogonal Slepian tapers to the data, where T is the duration of the data and W is the half bandwidth of the smoothing window, which we chose to be 5 Hz. The LFP signal was treated as a continuous signal and spike trains were treated as a discrete signal, binned with 1 ms resolution into a sequence of event times.

We evaluated spike-field coherence (SFC) by calculating the coherency,  $C_{xy}$ , as the cross-spectra between signals  $x$  and  $y$  ( $S_{xy}$ ) normalized by the geometric mean of their autospectra ( $S_{xx}$  and  $S_{yy}$ ):

$$C_{xy}(f) = \frac{S_{xy}(f)}{\sqrt{S_{xx}(f)S_{yy}(f)}} \quad (\text{Equation 1})$$

$C_{xy}$  is a complex number. Its modulus represents the value of coherence, which lies between 0 and 1. The phase of this complex number is the relative phase difference between the two signals.

We analyzed the phase of spikes with respect to the gamma cycle by using a fourth-order band-pass filter to isolate the 30–50 Hz frequency components of the LFP. We then applied the Hilbert transform to estimate the phase of this complex signal at each time instant, and counted the number of spikes occurring in each 45 degree bin. The preferred phase,  $\phi_{\text{pref}}$ , for each neuron was defined as

$$\phi_{\text{pref}} = \arctan \left( \frac{\sum_{n=1}^N R_n \sin(\phi_n)}{\sum_{n=1}^N R_n \cos(\phi_n)} \right), \quad (\text{Equation 2})$$

where  $R_n$  is the spike count of the  $n^{\text{th}}$  bin relative to the minimum spike counts across bins and  $\phi_n$  is the center phase of the  $n^{\text{th}}$  bin. We determined the clustering of spikes in the gamma cycle, or phase bias, as

$$\text{Bias} = \frac{\left| \sum_{n=1}^N R_n e^{i\phi_n} \right|}{\sum_{n=1}^N R_n} \quad (\text{Equation 3})$$

We calculated CCGs using standard methods, described in [Smith and Kohn \(2008\)](#). To correct for stimulus-locked correlations, we subtracted CCGs calculated from trial-shuffled data from the raw CCG. To isolate brief timescale correlation (synchrony), we subtracted from the raw CCG a predictor calculated from surrogate data in which spike times were jittered in a 25 ms window ([Smith and Kohn, 2008](#)). This corrects for both stimulus-locked correlations and slow fluctuations of responsivity. Both calculations were normalized by the firing rate of both cells. For V1-V2 pairs, we defined the jitter-corrected CCG to be significant if the peak within 10 ms of zero time lag was more than 5 standard deviations above the values at time lags of  $\pm 75$ –125 ms.

We rate matched responses across conditions using the approach of [Gregoriou et al. \(2009\)](#). For each stimulus condition, we calculated the peristimulus time histogram (PSTH) of each single unit or MUA cluster. At each 1 ms time epoch of the PSTH, we defined the weakest response across stimulus sizes for each orientation. We then calculated the difference between this response and each stronger response, divided by the stronger response. We used this scaling factor to delete spikes randomly from the stronger responses. For each orientation and each unit, the PSTH was thus matched (in each 1 ms bin) across stimulus sizes. For experiments in which the two sizes were presented in separate blocks, rates were matched using the same approach but using the population PSTH.

All indications of variance are standard errors of the mean, unless otherwise indicated. All tests of statistical significance are two-tailed t tests, unless otherwise indicated.

#### SUPPLEMENTAL INFORMATION

Supplemental Information includes eight figures and can be found with this article online at <http://dx.doi.org/10.1016/j.neuron.2012.12.036>.

#### ACKNOWLEDGMENTS

This work was supported by grants from the National Institutes of Health (EY016774 and P30HD071593) and Research to Prevent Blindness. We thank Douglas McLelland and Steve Gotts for comments on an earlier version of this manuscript. We thank Amin Zandvakili for help with V1-V2 recordings and analysis.

Accepted: December 11, 2012

Published: February 20, 2013

#### REFERENCES

- Akam, T., and Kullmann, D.M. (2010). Oscillations and filtering networks support flexible routing of information. *Neuron* 67, 308–320.
- Angelucci, A., and Bressloff, P.C. (2006). Contribution of feedforward, lateral and feedback connections to the classical receptive field center and extra-classical receptive field surround of primate V1 neurons. *Prog. Brain Res.* 154, 93–120.
- Atallah, B.V., and Scanziani, M. (2009). Instantaneous modulation of gamma oscillation frequency by balancing excitation with inhibition. *Neuron* 62, 566–577.
- Berens, P., Keliris, G.A., Ecker, A.S., Logothetis, N.K., and Tolias, A.S. (2008). Feature selectivity of the gamma-band of the local field potential in primate primary visual cortex. *Front. Neurosci.* 2, 199–207.
- Bruno, R.M., and Sakmann, B. (2006). Cortex is driven by weak but synchronously active thalamocortical synapses. *Science* 312, 1622–1627.
- Buschman, T.J., and Miller, E.K. (2007). Top-down versus bottom-up control of attention in the prefrontal and posterior parietal cortices. *Science* 315, 1860–1862.
- Castelo-Branco, M., Neuenschwander, S., and Singer, W. (1998). Synchronization of visual responses between the cortex, lateral geniculate nucleus, and retina in the anesthetized cat. *J. Neurosci.* 18, 6395–6410.
- Cohen, M.R., and Kohn, A. (2011). Measuring and interpreting neuronal correlations. *Nat. Neurosci.* 14, 811–819.
- Colgin, L.L., Denninger, T., Fyhn, M., Hafting, T., Bonnevie, T., Jensen, O., Moser, M.B., and Moser, E.I. (2009). Frequency of gamma oscillations routes flow of information in the hippocampus. *Nature* 462, 353–357.
- Engel, A.K., Kreiter, A.K., König, P., and Singer, W. (1991). Synchronization of oscillatory neuronal responses between striate and extrastriate visual cortical areas of the cat. *Proc. Natl. Acad. Sci. USA* 88, 6048–6052.
- Friedman-Hill, S., Maldonado, P.E., and Gray, C.M. (2000). Dynamics of striate cortical activity in the alert macaque: I. Incidence and stimulus-dependence of gamma-band neuronal oscillations. *Cereb. Cortex* 10, 1105–1116.
- Frien, A., Eckhorn, R., Bauer, R., Woelbern, T., and Kehr, H. (1994). Stimulus-specific fast oscillations at zero phase between visual areas V1 and V2 of awake monkey. *Neuroreport* 5, 2273–2277.
- Fries, P. (2009). Neuronal gamma-band synchronization as a fundamental process in cortical computation. *Annu. Rev. Neurosci.* 32, 209–224.
- Fries, P., Roelfsema, P.R., Engel, A.K., König, P., and Singer, W. (1997). Synchronization of oscillatory responses in visual cortex correlates with perception in interocular rivalry. *Proc. Natl. Acad. Sci. USA* 94, 12699–12704.
- Fries, P., Reynolds, J.H., Rorie, A.E., and Desimone, R. (2001). Modulation of oscillatory neuronal synchronization by selective visual attention. *Science* 291, 1560–1563.
- Fries, P., Womelsdorf, T., Oostenveld, R., and Desimone, R. (2008). The effects of visual stimulation and selective visual attention on rhythmic neuronal synchronization in macaque area V4. *J. Neurosci.* 28, 4823–4835.
- Fröhlich, F., and McCormick, D.A. (2010). Endogenous electric fields may guide neocortical network activity. *Neuron* 67, 129–143.
- Gieselmann, M.A., and Thiele, A. (2008). Comparison of spatial integration and surround suppression characteristics in spiking activity and the local field potential in macaque V1. *Eur. J. Neurosci.* 28, 447–459.
- Girard, P., and Bullier, J. (1989). Visual activity in area V2 during reversible inactivation of area 17 in the macaque monkey. *J. Neurophysiol.* 62, 1287–1302.
- Girard, P., Hupé, J.M., and Bullier, J. (2001). Feedforward and feedback connections between areas V1 and V2 of the monkey have similar rapid conduction velocities. *J. Neurophysiol.* 85, 1328–1331.
- Gray, C.M. (1999). The temporal correlation hypothesis of visual feature integration: still alive and well. *Neuron* 24, 31–47, 111–125.

- Gray, C.M., and Singer, W. (1989). Stimulus-specific neuronal oscillations in orientation columns of cat visual cortex. *Proc. Natl. Acad. Sci. USA* **86**, 1698–1702.
- Gray, C.M., König, P., Engel, A.K., and Singer, W. (1989). Oscillatory responses in cat visual cortex exhibit inter-columnar synchronization which reflects global stimulus properties. *Nature* **338**, 334–337.
- Gregoriou, G.G., Gotts, S.J., Zhou, H., and Desimone, R. (2009). High-frequency, long-range coupling between prefrontal and visual cortex during attention. *Science* **324**, 1207–1210.
- Haider, B., Krause, M.R., Duque, A., Yu, Y., Touryan, J., Mazer, J.A., and McCormick, D.A. (2010). Synaptic and network mechanisms of sparse and reliable visual cortical activity during nonclassical receptive field stimulation. *Neuron* **65**, 107–121.
- Hasenstaub, A., Shu, Y., Haider, B., Kraushaar, U., Duque, A., and McCormick, D.A. (2005). Inhibitory postsynaptic potentials carry synchronized frequency information in active cortical networks. *Neuron* **47**, 423–435.
- Ito, J., Maldonado, P., Singer, W., and Grün, S. (2011). Saccade-related modulations of neuronal excitability support synchrony of visually elicited spikes. *Cereb. Cortex* **21**, 2482–2497.
- Jia, X., Smith, M.A., and Kohn, A. (2011). Stimulus selectivity and spatial coherence of gamma components of the local field potential. *J. Neurosci.* **31**, 9390–9403.
- Jia, X., Xing, D., and Kohn, A. (2013). No consistent relationship between gamma power and peak frequency in macaque primary visual cortex. *J. Neurosci* **33**, 17–25.
- Kayser, C., Salazar, R.F., and König, P. (2003). Responses to natural scenes in cat V1. *J. Neurophysiol.* **90**, 1910–1920.
- Kohn, A., Zandvakili, A., and Smith, M.A. (2009). Correlations and brain states: from electrophysiology to functional imaging. *Curr. Opin. Neurobiol.* **19**, 434–438.
- Lima, B., Singer, W., Chen, N.H., and Neuenschwander, S. (2010). Synchronization dynamics in response to plaid stimuli in monkey V1. *Cereb. Cortex* **20**, 1556–1573.
- Montemurro, M.A., Rasch, M.J., Murayama, Y., Logothetis, N.K., and Panzeri, S. (2008). Phase-of-firing coding of natural visual stimuli in primary visual cortex. *Curr. Biol.* **18**, 375–380.
- Montgomery, S.M., and Buzsáki, G. (2007). Gamma oscillations dynamically couple hippocampal CA3 and CA1 regions during memory task performance. *Proc. Natl. Acad. Sci. USA* **104**, 14495–14500.
- Nelson, M.J., Pouget, P., Nilsen, E.A., Patten, C.D., and Schall, J.D. (2008). Review of signal distortion through metal microelectrode recording circuits and filters. *J. Neurosci. Methods* **169**, 141–157.
- Pesaran, B., Pezaris, J.S., Sahani, M., Mitra, P.P., and Andersen, R.A. (2002). Temporal structure in neuronal activity during working memory in macaque parietal cortex. *Nat. Neurosci.* **5**, 805–811.
- Ray, S., and Maunsell, J.H. (2010). Differences in gamma frequencies across visual cortex restrict their possible use in computation. *Neuron* **67**, 885–896.
- Ray, S., and Maunsell, J.H. (2011). Different origins of gamma rhythm and high-gamma activity in macaque visual cortex. *PLoS Biol.* **9**, e1000610.
- Reyes, A.D. (2003). Synchrony-dependent propagation of firing rate in iteratively constructed networks in vitro. *Nat. Neurosci.* **6**, 593–599.
- Rockland, K.S. (1992). Laminar distribution of neurons projecting from area V1 to V2 in macaque and squirrel monkeys. *Cereb. Cortex* **2**, 38–47.
- Salinas, E., and Sejnowski, T.J. (2001). Correlated neuronal activity and the flow of neural information. *Nat. Rev. Neurosci.* **2**, 539–550.
- Samonds, J.M., and Bonds, A.B. (2005). Gamma oscillation maintains stimulus structure-dependent synchronization in cat visual cortex. *J. Neurophysiol.* **93**, 223–236.
- Schmid, M.C., Panagiotaropoulos, T., Augath, M.A., Logothetis, N.K., and Smirnakis, S.M. (2009). Visually driven activation in macaque areas V2 and V3 without input from the primary visual cortex. *PLoS ONE* **4**, e5527.
- Singer, W. (1999). Neuronal synchrony: a versatile code for the definition of relations? *Neuron* **24**, 49–65, 111–125.
- Smith, M.A., and Kohn, A. (2008). Spatial and temporal scales of neuronal correlation in primary visual cortex. *J. Neurosci.* **28**, 12591–12603.
- Smith, M.A., Jia, X., Zandvakili, A., and Kohn, A. (2012). Laminar dependence of neuronal correlations in visual cortex. *J. Neurophysiol.* Published online November 28, 2012. <http://dx.doi.org/10.1152/jn.00846.2012>.
- Van Essen, D.C., Newsome, W.T., and Maunsell, J.H. (1984). The visual field representation in striate cortex of the macaque monkey: asymmetries, anisotropies, and individual variability. *Vision Res.* **24**, 429–448.
- Whittington, M.A., Cunningham, M.O., LeBeau, F.E., Racca, C., and Traub, R.D. (2011). Multiple origins of the cortical  $\gamma$  rhythm. *Dev. Neurobiol.* **71**, 92–106.
- Womelsdorf, T., Schoffelen, J.M., Oostenveld, R., Singer, W., Desimone, R., Engel, A.K., and Fries, P. (2007). Modulation of neuronal interactions through neuronal synchronization. *Science* **316**, 1609–1612.
- Zeitler, M., Fries, P., and Gielen, S. (2006). Assessing neuronal coherence with single-unit, multi-unit, and local field potentials. *Neural Comput.* **18**, 2256–2281.